Chemical Science

Accepted Manuscript

This article can be cited before page numbers have been issued, to do this please use: S. Bedajna, K. G. Reynolds, M. Karimi, E. Litle, D. G. Nocera and F. P. Gabbaï, *Chem. Sci.*, 2026, DOI: 10.1039/D6SC01586G.

ROYAL SOCIETY OF CHEMISTRY

rsc.li/chemical-science

View Article Online
DOI: 10.1039/D6SC01586G

ARTICLE

Visible-Light-Induced Chlorine Photoelimination from Acridinium-Phosphine Gold(III) Complexes

Received 00th January 20xx,
Accepted 00th January 20xx

DOI: 10.1039/x0xx00000x

Shantabh Bedajna[a], Kristopher G. Reynolds[b], Mohammadjavad Karimi[a], Elishua Litle[a], Daniel G. Nocera*[b], and François P. Gabbaï*[a]

With the objective of developing transition metal complexes that undergo visible-light-induced halogen photoelimination, we have successfully synthesized trivalent gold trichloride complexes featuring an acridinium unit. Photoexcitation of the acridinium π^+ system with green light allows for facile photoreduction to the corresponding Au^I complexes, highlighting the photolability imparted by this moiety onto the Au^{III} center. The photolysis is remarkably clean, particularly in the solid state where the photodechlorination is essentially trap-free. Transient absorption spectroscopic studies reveal that the photochemistry is derived from a pathway whereby the S1 excited state of the acridinium undergoes energy transfer to the Au^{III} center to prompt the photogeneration of Cl radicals.

Introduction

In the past two decades, light-induced processes have found increasing importance in the production of fuels as well as organic synthesis.[1] Photoinduced halogen evolution in particular has been rigorously investigated as an appealing approach to close the oxidative side of HX splitting cycles.[2] Often referred to as the bottleneck of this energy conversion scheme,[3] Cl_2 elimination has enjoyed much attention from the scientific community. A number of strategies have thus emerged to investigate this process, with the simplest being exemplified by transition metal complexes, such as **A** and **B** (Figure 1), which undergo net Cl_2 loss upon photoexcitation to ^{3}LMCT states with weakened M–Cl bonds.[4] High valent gold complexes have also been considered for such processes as described in some of our earlier contributions.[4c, 5] For example, $(Ph_3P)AuCl_3$ **C** undergoes photoreduction to its gold monochloride counterpart with quantum yields in the 11-13% range when irradiated at 320 nm.[4c] Based on the notion that such chemistry could, in principle, be driven from an organic chromophore that absorbs near or in the visible range, additional strategies have been considered as in the case of systems of type **D** in which ambient light harvested by the diphenylanthracene chromophore induces photoreduction, even though this process is more efficient upon irradiation at 365 nm.[6]

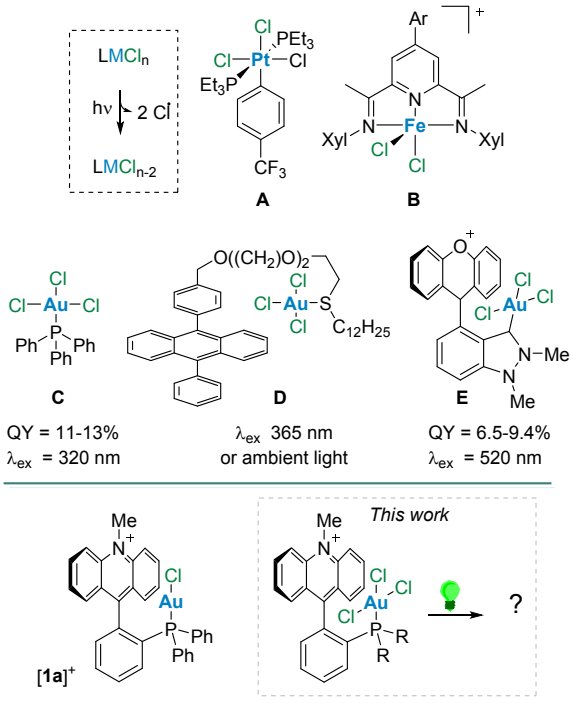

Figure 1 Top: General photoreductive chlorine elimination and relevant examples of systems that support this transformation. Bottom: Structure of a relevant phosphine-acridinium gold complex and graphical representation of the idea explored in this paper.

Building on these precedents, we have started to target platforms that incorporate cationic heteroanthracene moieties. Our strategy rests on the notion that the visible absorption profile of such chromophores would provide a low-energy entrance channel for the targeted photoreductive process. We also speculated that, if placed near the metal centre, such cationic aromatic moieties would preferentially stabilize the low valent form of the metal via [M]···π^+ interactions, providing an impetus for the reduction. In a first implementation of this idea,

[a] Department of Chemistry, Texas A&M University, College Station, TX 77843, USA. E-mail: francois@tamu.edu
[b] Department of Chemistry and Chemical Biology, Harvard University, 12 Oxford Street, Cambridge, MA 02138, USA
† Electronic supplementary information (ESI) available: Additional experimental and computational details. CCDC 2521156-2521158. For ESI and crystallographic data in CIF or other electronic format see XXXXXXXXXXX

View Article Online DOI: 10.1039/D5SC01586G

we recently reported **E**, a gold(III) complex decorated with an adjacent xanthylium unit.[7] We showed that excitation of this derivative, using green light, results in both a xanthylium-

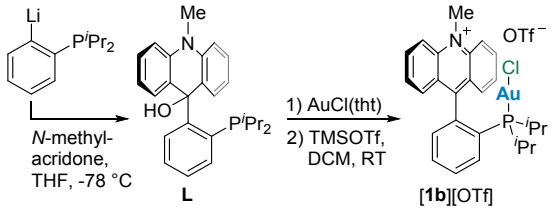

Scheme 1 Synthesis of [**1b**][OTf].

centred π→π* excitation and an intramolecular charge transfer excitation from the indazole backbone to the xanthylium π* orbital. Access to these two excited states was correlated to the clean dechlorination that ensues at the gold centre.

Aiming to test whether such a strategy could also be implemented in phosphine-based platforms, we have now decided to target phosphine gold(III) complexes that incorporate the *N*-methylacridinium chromophore. This chromophore, which is found in several photocatalysts as originally described by Fukuzumi,[8] is appealing because of its chemical resilience to both reductive[9] and oxidative processes.[10] Moreover, we have already shown that it could be incorporated in phosphine gold(I) derivatives such as [**1a**]$^+$,[11] providing a logical starting point for this investigation. In this contribution, we describe our efforts towards the synthesis and photochemistry of trivalent analogs of gold complexes such as [**1a**]$^+$ along with an investigation of relevant excited states dynamics using transient absorption techniques.

Results and discussion

Synthesis and structural analyses of the complexes

In addition to using complex [**1a**]$^+$ as a starting point for these studies, we also considered its diisopropyl analog [**1b**]$^+$, which was prepared for the purpose of this study (Scheme 1). This new derivative was accessed from (2-lithiophenylene) diisopropylphosphine which was quenched with *N*-methylacridone to afford a carbinol (**L**) that was aurated with AuCl(tht) (tht = tetrahydrothiophene) and dehydroxylated using TMSOTf (Scheme 1). Unlike its diphenylphosphino analog, [**1b**][OTf] is a mildly air-sensitive salt that displays a single resonance in the ^{31}P[12] NMR spectrum at 48.4 ppm, similar to the chemical shift of 51.8 ppm reported for [(Ph^{i}Pr$_2$P)AuCl],[13] suggesting the formation of the desired cationic gold(I) complex [**1b**][OTf]. Indeed, ^{13}C{^{1}H} NMR spectroscopy provided confirmation of the cationic nature of this molecule, showing the carbenium resonance at 160.6 ppm, similar to the 159.7 ppm reported for [**1a**]$^+$.[11a] Single crystal X-ray diffraction analysis of this complex verified the structure of this derivative (Figure 2), revealing that the AuCl unit is oriented toward the cationic π$^+$ surface of acridinium, similar to that observed for [**1a**]$^+$.[11a] The Au–mpln$_{acr}$ and Cl–mpln$_{acr}$ (mpln$_{acr}$ = acridinium moiety mean plane) distances in [**1b**]$^+$ at 3.154(4) Å and 3.508(6) Å, respectively, are slightly longer than the analogous distances

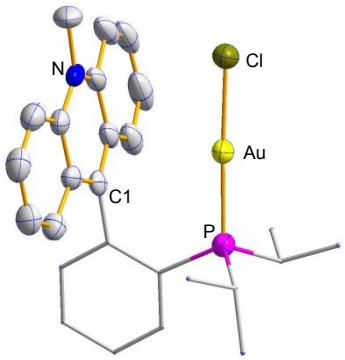

Figure 2 Solid state structure of [**1b**][OTf]. Thermal ellipsoids are drawn at the 50% probability level and hydrogen atoms and counterions are omitted for clarity. Relevant metrical parame-ters are in the main text

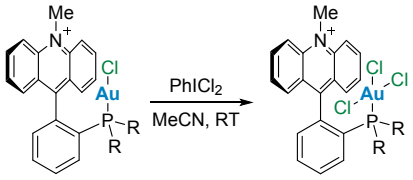

Scheme 2 Synthesis of the gold(III) derivatives.

in [**1a**]$^+$ at 3.043(4) Å and 3.318(5) Å. The Au–C1 distance at 3.141(11) Å is slightly shorter than the analogous distance in [**1a**]$^+$ at 3.168(9) Å. However, NBO analysis on the optimized structure of this derivative did not identify any significant interactions between the Au atom and C1. The observed orientation, with the AuCl moiety upright with respect to the acridinium unit, is most likely the result of favorable electrostatic AuCl···π$^+$ interactions as described previously in the case of [1a]+ [11b]and related complexes.[11d]

The target gold(III) complexes could be conveniently obtained by chlorination of [**1a**]$^+$ and [**1b**]$^+$ using PhICl$_2$ (Scheme 2). ^{31}P{^{1}H} NMR analysis of these reaction mixtures shows quantitative conversion of the gold(I) species and the appearance of new signals downfield shifted from the starting materials at 42.7 ppm and 63.0 ppm for [**2a**]$^+$ and [**2b**]$^+$, respectively. The chemical shift of [**2a**]$^+$ is reminiscent of that reported for [Ph$_3$PAuCl$_3$] at 43.9 ppm,[4c] suggesting successful oxidation to the gold centre. ^{13}C{^{1}H} NMR analysis of these products indicated the retention of the acridinium unit, noted by a characteristic carbenium signal at 157.3 ppm for both derivatives. Diffusion of Et$_2$O into concentrated solutions of these salts in MeCN afforded single crystals suitable for X-ray analysis. In the solid state, both complexes show square planar geometry around the gold atom and have similar bond distances (Figure 3). For [**2a**]$^+$, The Au–Cl2 bond distance of 2.3320(12) Å is slightly longer than the Au–Cl1 and Au–Cl3 distances of 2.2723(13) Å and 2.2956(13) Å respectively, consistent with the more substantial trans influence of the phosphine ligand. These structures, however, differ significantly in the orientation of the AuCl$_3$ moiety relative to the acridinium π$^+$ surface. While the AuCl$_3$ moiety in [**2a**]$^+$ is positioned away from the π$^+$ system (Cl1–mpln$_{acr}$ distance = 5.625(6) Å, Au–mpln$_{acr}$ distance = 3.991(6) Å), the same

View Article Online
DOI: 10.1039/D6SC01586G

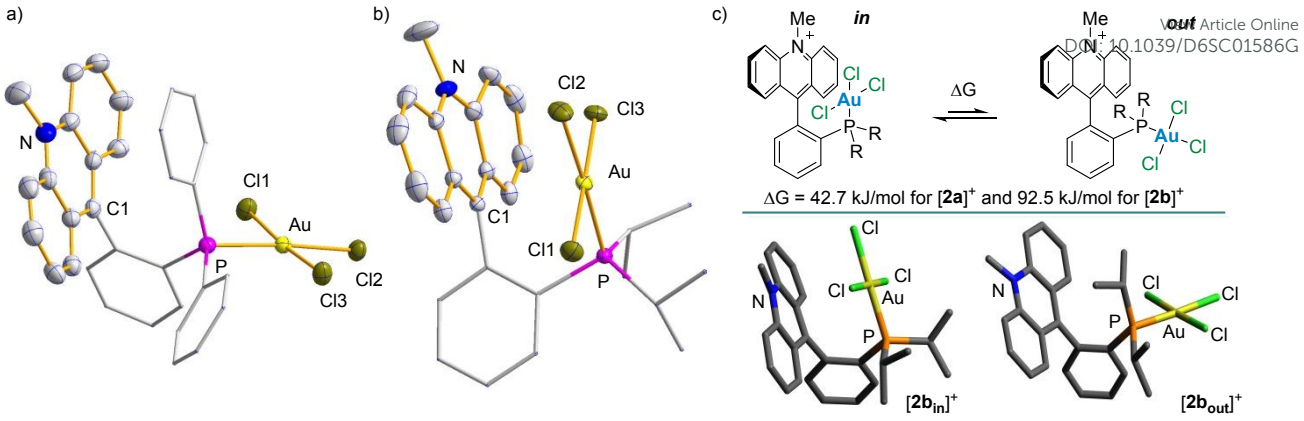

Figure 3 a) Solid state structure of [**2a**][BF4] b) Crystal structure of [**2b**][OTf] Thermal ellipsoids are drawn at the 50% probability level and hydrogen atoms and counterions are omitted for clarity. c) "In/out" equilibrium and optimized structures of the two conformers of [**2b**]$^+$ obtained from DFT calculations at the MPW1PW91/mixed basis set level of theory.

fragment in [**2b**]$^+$ retains its upright orientation and remains in contact with the acridinium unit, as indicated by the Au–mpln$_{acr}$ and Cl1–mpln$_{acr}$ distances of 3.2182(19) Å and 3.6525(19) Å, respectively.

This conformational difference urged us to explore the conformations of these gold(III) complexes computationally. Density Functional Theory (DFT) calculations carried out using the MPW1PW91 functional and a mixed basis set (cc-pVTZ-PP for Au; 6-31G(d',p') for P/Cl; 6-31G(d') for C/N; 6-31G for H) unveiled two local minima corresponding to two conformers with the $AuCl_3$ moiety drawn inward [**2b**$_{in}$]$^+$ or oriented away [**2b**$_{out}$]$^+$ from the acridinium surface (Figure 3c). Interestingly, the inward conformer [**2b**$_{in}$]$^+$ is 92.5 kJ mol^{-1} lower in Gibbs free energy than the outward conformer [**2b**$_{out}$]$^+$. Similar calculations on [**2a**]$^+$ also revealed two conformers, with the inward conformer [**2a**$_{in}$]$^+$ lying 42.7 kJ mol^{-1} lower in Gibbs free energy than [**2a**$_{out}$]$^+$. These calculations suggest that the smaller energy difference between the two conformers of [**2a**]$^+$ may be more easily overcome by energetically favorable lattice effects, which are elevated by the fact that these complexes are isolated as salts. In either case, the global minimum on the energy surface is the inward conformer with the $AuCl_3$ core situated in the proximity of the acridinium chromophore. This arrangement, which we thought might elevate the photolability of the chloride ligands,[14] is much like the gold-based systems featuring ambiphilic ligands that interact with the AuCl moiety.[15]

Photophysical properties and photochemistry

Eager to investigate this possibility, we decided first to study these complexes by UV-vis spectroscopy. The most salient feature of the spectra of these gold derivatives is the presence of broad low-energy absorption bands in the 390-490 nm region (Figure 4a, Figure S10-S12). These bands closely resemble those of simple 9-aryl-*N*-methylacridinium compounds,[11b, 16] indicating the unambiguous contribution of the acridnium-centred π→π* excitation to this feature. To support this assumption and identify other possible contributors, we carried out Time Dependent (TD) DFT using the "in" conformers of [**2a**]$^+$ and [**2b**]$^+$. These calculations reveal the primary contributions of two excitations, which both involve the HOMO, LUMO and LUMO+1 (Figure S30-S32, Table S3-S5). Because the LUMO and LUMO+1 show dominant acridinium π* and Au–Cl σ* (d_{x2-y2}) character, respectively, the first excitation (E_a) has dominant π→π* excitation character, while the second one (E_b) has mainly π→Au–Cl σ* ($d_{x^2-y^2}$) character (Figure 4b). Carrying out these calculations on the "out" conformers affords very similar results, with two low-energy excitations of analogous orbital parentage. These computational findings pose the possibility of Cl$^\bullet$ dissociation either by weakened Au–Cl bonds in the excited state due to population of the Au–Cl σ* orbital or by direct

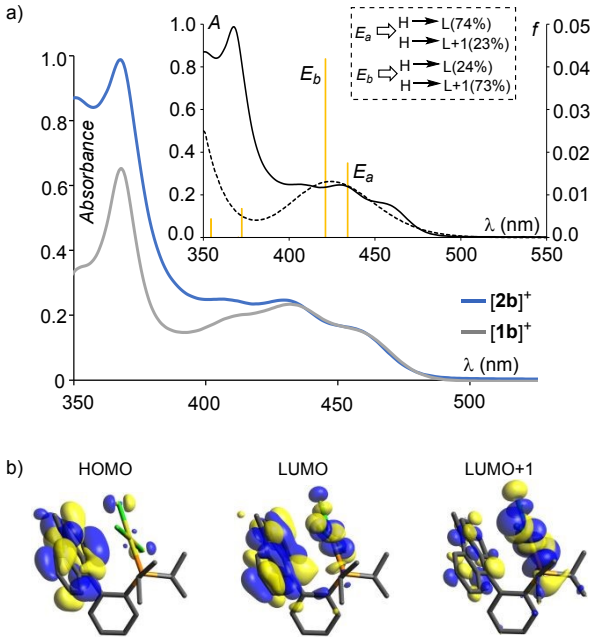

Figure 4 a) UV-vis spectra of 10-5 M solutions of [**2b**]$^+$ and [**1b**]$^+$ in MeCN. The inset shows the experimental (solid) and predicted (dashed) UV-vis spectra of [**2b**$_{in}$]$^+$ overlaid with the TD-DFT calculated vertical excitations (yellow bars). b) Orbitals in-volved in the vertical excitations (drawn at 0.05 isosurface value).

View Article Online
DOI: 10.1039/D6SC01586G

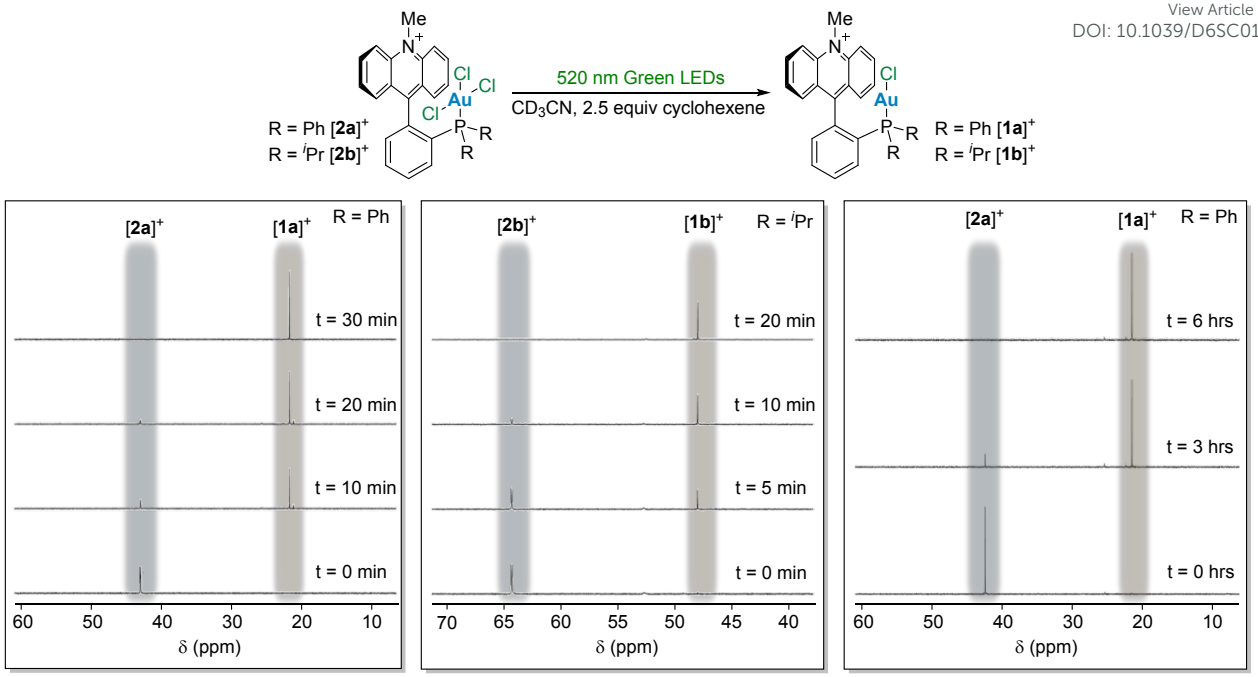

Figure 5 ^{31}P NMR monitored photoreductive elimination of chlorine from a 0.02 M solution of [**2a**]$^+$ (left) and [**2b**]$^+$ (middle), both in the presence of 0.05 M cyclohexene as a chlorine trap and H_3PO_4 in a sealed capillary as an internal standard, using 5 W green LEDs as the light source. The right panel shows the ^{31}P NMR monitored photoreductive elimination of chlorine from [**2a**]$^+$ in the solid state.

energy transfer from the excited acridinium chromophore to the trivalent gold moiety. Targeting reductive elimination from gold(III),[17] such a possibility has recently been taken advantage of to afford fluoroarenes.[18]

We next turned our attention to the photochemistry of [**2a**]$^+$ and [**2b**]$^+$ using a commercial green light source characterized by a relatively broad illumination spectrum , similar to previous work on hydrohalic acid splitting using non-monochromatic light.[19] The full width at half maximum (30 nm) of this light source, centred at 520 nm, is sufficiently broad to overlap with the low-energy tail of the acridinium absorption envelope of these two compounds (Figure S13). Irradiation of [**2a**]$^+$ and [**2b**]$^+$ in MeCN in the presence of 2.5 equiv. of cyclohexene as a chlorine trap resulted in the rapid photoreduction of the gold centre, as indicated by ^{31}P NMR spectroscopy which showed the progressive disappearance of the gold(III) complexes [**2a**]$^+$ and [**2b**]$^+$ in concert with the emergence of their gold(I) counterparts [**1a**]$^+$ and [**1b**]$^+$ (Figure 5, Figure S16-S17). The photolysis was complete after 20 minutes, and integration of the peaks with respect to the internal standard H_3PO_4, implemented as a sealed capillary in the NMR tube, showed negligible loss of material, indicating that the photoreduction of these complexes is not significantly affected by decomposition of these systems through side reactions. Interestingly, the photolysis of both compounds without a trap proceeds in a clean fashion as well, albeit at a slower rate (Figure S14-S15). Encouraged by the resilience of these systems, we selected [**2a**]$^+$ for further investigation in the solid state. To this end, [**2a**][BF_4] was dissolved in MeCN and drop-cast on a glass slide. While irradiating this compound in air for 60 min followed by dissolution in CD_3CN showed conversion into [**1a**][BF_4], signs of photodecomposition were also present. Carrying out the same reaction in a N_2-filled glovebox circumvented this issue, furnishing much cleaner conversion of [**2a**]$^+$ and [**2b**]$^+$ into [**1a**]$^+$ and [**1b**]$^+$ respectively (Figure 5, Figure S19-S20), further documenting the remarkable resilience of the platform. This experiment provides a rare example of solid-state photoreductive elimination of a halogen, with other examples seen in the Fe^{III} complex **B**,[4f] the dimeric Pt^{III}–Pt^{III} complex **F**,[20] the heterobimetallic [PtSb]^{VII} molecule **G**,[21] the dinuclear gold derivative **H**,[4c] and the Ni^{III} system **I** (Figure 6).[22] These

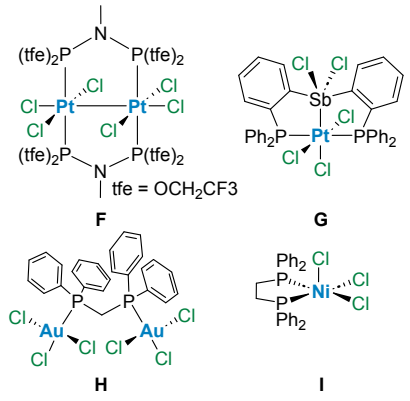

Figure 6 Known examples of complexes supporting solid state photo-elimination of halogens.

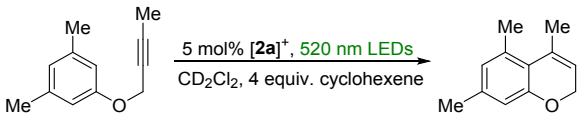

Scheme 3 Gold-catalysed hydroarylation of alkynes turned on by the photolysis of [**2a**][BF4].

complexes photoeliminate halogen equivalents upon irradiation with higher energy UV light, leading to the formation of undesired decomposition products. Such side reactions appear to be much less prevalent in the case of [**2a**][BF_4], which, incidentally, might be the only metal platform known to this day to photoeliminate chlorine in the solid state using visible light. The clean photoinduced dechlorination of [**2a**]$^+$ into [**1a**]$^+$ led us to consider whether the scope of this photolysis reaction could be expanded to application in organometallic catalysis.[23] The photoevolution of chlorine radicals should produce HCl via C-H bond activation a suitable trap as previously proposed for similar complexes.[7] We questioned whether the released acid and the formation of [**1a**]$^+$ by irradiation of [**2a**]$^+$ would produce a catalytically competent system in which the Au-Cl bond of [**1a**]$^+$ is activated by hydrogen bonding with the released acid.[24] We decided to test this idea using the known intramolecular hydroarylation of **3** as a test reaction.[25] When this compound was irradiated in the presence of [**2a**]$^+$ (5%) and cyclohexene (20%) as a chlorine trap using the above mentioned 520 nm LED light, 47% conversion to the hydroarylation product **4** was observed by ^{1}H NMR after 30 minutes (Scheme 3, Figure S26). No catalysis was observed in the absence of light. This simple experiment shows that carbophilic catalysis can be activated by *in situ* photoreduction of [**2a**]$^+$. These results parallel those obtained with complexes such as **D**, which also afford catalytically active systems that readily promote the isomerization of propargyl amides.[6]

Quantum yield measurements with azobenzene as the chemical actinometer[26] and monitored by ^{1}H and ^{31}P NMR spectroscopy (Figure S21) show that the photoreduction of [**2a**]$^+$ and [**2b**]$^+$ proceeds with quantum yields of 6.1 % and 7.9 %, respectively, when 2.5 equiv. of cyclohexene is employed. These quantum yields increase to 18.9 % and 20.5 % when the trap concentration is raised to 25 equiv. (Table S1-S2). The elevated magnitude of these quantum yields shows that these systems are among the most active platforms for light-induced chlorine evolution.

These unique photochemical features spark questions about the mechanism of chlorine elimination from the Au(III) platform. There are two possible pathways for net Cl_2 elimination: (i) concerted reductive elimination of a Cl_2 molecule, and (ii) stepwise dissociation of two Cl$^\bullet$ radicals. Our TD-DFT analyses indicate that the radical mechanism is favored (*vide supra*). GC-MS analysis of an irradiated solution of [**2a**]$^+$ in the presence of 10 equiv. of cyclohexene showed formation of 3-chlorocyclohexene along with other unidentified products (Figure S18). These results suggest the involvement of Cl$^\bullet$ radicals, although the concerted formation of Cl_2 cannot be entirely ruled out, given the complex mixture of products suggested by the gas chromatogram. To delineate the underlying photophysical process leading to chlorine elimination, we examined [**2a**]$^+$ and its photoproduct [**1a**]$^+$ via transient absorption spectroscopy (TA) on both femto- and nanosecond timescales.

View Article Online DOI: 10.1039/D5SC01586C

Transient absorption spectroscopy

For context, the photophysics and photochemistry of acridinium dyes have been extensively investigated.[27] The excited state dynamics in acridinium dyes substituted at the 9 position are generally governed by two pathways arising from whether substituents on the dye are able to be oxidized by the acridinium singlet excited state (charge transfer in nature) or not (π localized in nature). The latter exhibits relatively simple photophysics;[28] population of the acridinium-centred singlet excited state is followed by direct return to the ground state, typically by radiative relaxation.[27b] When substituents of the dye are able to be oxidized, rapid charge transfer occurs from the singlet excited state, leading to the formation of the acridinyl radical and the radical cation on the substituent. The absorption spectrum of the resulting acridinyl radical is marked by a characteristic broad band between 500-550 nm. To our knowledge, in all cases where intramolecular charge transfer is observed, charge recombination occurs on the nanosecond timescale to form the acridinium triplet excited state with its subsequent relaxation to the ground state.[27b, 28]

To elucidate the excited state dynamics governing the photochemical conversion of [**2a**]$^+$ to [**1a**]$^+$, we first established the photophysics of the [**1a**]$^+$ photoproduct. Figure S22a shows the femtosecond TA (fsTA) profile of [**1a**]$^+$. Immediately upon excitation (λ_{exc} = 420 nm, 60 nJ), two prominent Excited State Absorptions (ESAs) of the singlet excited state are observed at 395 nm and 480 nm, in addition to a broad ESA extending from 650 nm to the edge of our probe region in the near-infrared (NIR). The bleach feature at 550 nm is attributable to stimulated emission from the singlet excited state. This singlet excited state evolves with a time- constant of 54 ps (Figure S22b) to the characteristic acridinium triplet excited state, which persists longer than our 6 ns delay line. This localized triplet excited state is captured on our nanosecond TA (nsTA) system (Figure S22c), and it decays to baseline with a time-constant of 408 ns (Figure S22d). These data establish that the singlet state of [**1a**]$^+$ undergoes rapid intersystem crossing to the localized acridinium triplet state, mediated by the large spin-orbit coupling induced by the Au(I) centre, followed by straightforward decay to the ground state.

The coordination of P to the gold centre prevents its oxidation by the acridinium singlet excited state. Figure S23 shows the fsTA spectrum of the ligand species [(*o*-$Ph_2P(C_6H_4)$Acr)]$^+$ ([Acr = 9-*N*-methylacridinium) also referred to as EliPhos.[29] Laser excitation at λ_{exc} = 425 nm produces a prompt TA spectrum that is dominated by the intense absorption signal at λ > 475 nm that is characteristic of the acridinyl radical.[11b] Unbound to gold, the lone pair of P is readily photooxidized by intramolecular electron transfer. We note that the acridinyl radical absorption

View Article Online DOI: 10.1039/D6SC01586C

spectrum is absent in the TA spectroscopy of [**1a**]$^+$, thus establishing that CT does not occur between the singlet excited state and the Au(I) centre.

Femtosecond TA experiments on [**2a**]$^+$ are very similar to those of [**1a**]$^+$. The singlet excited state forms immediately upon excitation (λ_{exc} = 420 nm, 115 nJ) with the same

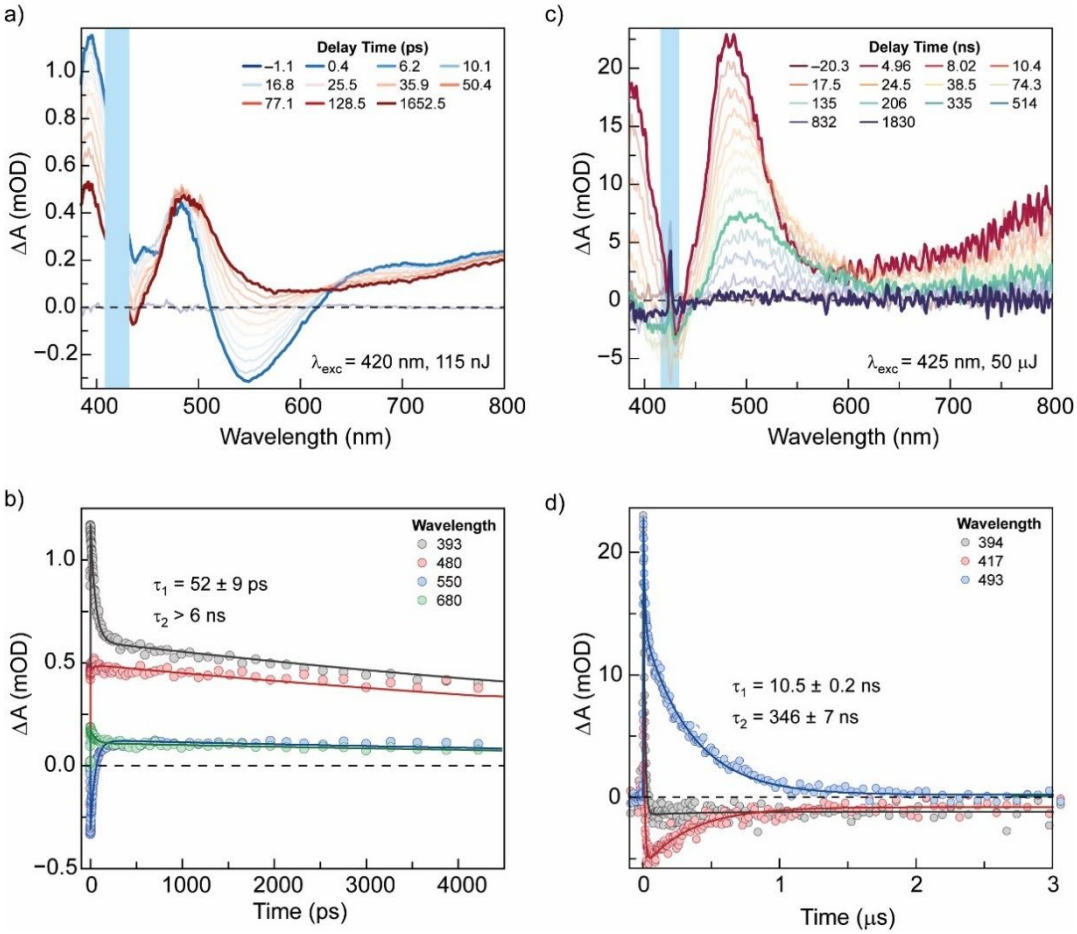

Figure 7 a) Femtosecond TA spectra of 114 μM [**2a**]$^+$ in MeCN. b) Femtosecond TA kinetics of [**2a**]$^+$ in MeCN. c) Nanosecond TA spectra of 114 μM [**2a**]$^+$ in MeCN . d) Nanosecond TA kinetics of [**2a**]$^+$ in MeCN.

characteristic ESAs at 395 nm and 480 nm and a broad ESA extending from 650 nm, along with a stimulated emission feature from the singlet excited state at 550 nm (Figure 7a). The 52-ps time evolution of the singlet in [**2a**]$^+$ (Figure 7b) is also the same as [**1a**]$^+$. However, the fsTA spectra of [**2a**]$^+$ notably differ from [**1a**]$^+$ in that the 395-nm feature of [**2a**]$^+$ is roughly half the intensity of that observed in the TA spectrum of [**1a**]$^+$. The spectrum decays with a time constant of 10.5 ns to reveal the triplet excited state, which then decays with its characteristic long lifetime of 346 ns. In contrast to [**1a**]$^+$, the nsTA thus establishes the generation of an additional intermediate from the singlet excited state of [**2a**]$^+$. The nanosecond TA spectrum of [**2a**]$^+$ (Figure 7c), as in [**1a**]$^+$, is that of the localized triplet excited state of acridinium and decays with a time-constant of 345 ns leaving a low intensity permanent bleaching feature between 380-500 nm that resembles the difference absorption spectrum of [**2a**]$^+$ and [**1a**]$^+$ (Figure S24), consistent with the photochemical conversion of [**2a**]$^+$ into [**1a**]$^+$. As was the case in [**1a**]$^+$, spectral features of the acridinyl radical, which would result from charge transfer, are absent throughout the entire dataset. Inasmuch as CT is not observed for the more easily oxidized Au(I) centre in [**1a**]$^+$, the lack of CT involving the Au(III) centre in [**2a**]$^+$ is unsurprising. Focusing on the intermediate uncovered in the 390-nm spectral region, the TA signal at 390 nm is quenched by cyclohexene with a diffusion limited quenching rate constant of $k_q = 1.1 \times 10^9$ $M^{-1}s^{-1}$ (Figure S25). Conversely, the lifetime of the triplet excited state, monitored at 483 nm, is unaffected by the presence of cyclohexene. This observation supports the TD-DFT and photochemical analyses (*vide supra*) that Cl$^\bullet$ is produced as a primary photoproduct, as cyclohexene is a known trap of Cl$^\bullet$. Accordingly, we believe that the unique intermediate produced from the singlet of [**2a**]$^+$, is a dissociated Cl$^\bullet$ residing in a solvent cage of the gold complex.[30] The decay time constant of 10.5 ns for this species is consistent with observed recombination rates of solvent-caged radicals in polar, organic solvents.[31]

Taken together, our data suggest the Jablonski diagrams shown in Figure 8 for [**1a**]$^+$ and [**2a**]$^+$. [**1a**]$^+$ shows simple photophysics of acridinium dyes in the presence of a heavy atom to induce intersystem crossing from the excited state singlet to triplet. Excitation of [**2a**]$^+$ leads to the population of an acridinium-centred singlet excited state with a rate constant for intersystem crossing that is similar to [**1a**]$^+$, as Au(I) and Au(III) are expected to have similar

spin-orbit coupling constants. Unlike [**1a**]$^+$, however, the singlet decays along a bifurcated pathway in which intramolecular energy transfer from the acridinium triplet to the Au(III)Cl_3 centre is competitive with intersystem crossing to lead to the generation of Cl$^\bullet$ within a solvent cage. We envision the generation of Cl$^\bullet$ to occur by energy transfer according to two possible pathways: (1) energy transfer into a dissociative d-d state to produce Au(III) and Cl^-, which is then subsequently oxidized within the solvent cage to produce [Au(II)Cl_2---Cl$^\bullet$] or alternatively energy transfer to a Au(III)---Cl^- LMCT state to produce [Au(II)Cl_2---Cl$^\bullet$]. Given that neither acridinium or the Au(III) center is sufficiently oxidizing to produce Cl$^\bullet$ from Cl^-, we believe relaxation through a LMCT state is the most likely pathway along which [Au(II)Cl_2---Cl$^\bullet$] forms. As shown in Figure 7c, this photoproduct dominates the initial nsTA spectrum at early times. Recombination of the radical within the solvent cage pair with a time constant of 10.5 ns reveals the underlying TA spectrum of the triplet excited state. Minor amounts of cage escape leads ultimately to the conversion of [**2a**]$^+$ into [**1a**]$^+$ via the loss of an additional Cl$^\bullet$ to result in the complete photochemical transformation.

Identification of energy transfer in [**2a**]$^+$ as the prevailing mechanism for the photochemical production of Cl$^\bullet$ is supported by the lack of a similar reactivity of [**1a**]$^+$. The Au(I) centre of [**1a**]$^+$ obviates energy transfer from the acridinium singlet to the gold centre, as d-d states are not present for a d^{10} electronic configuration. Thus, the Au(I) centre induces intersystem crossing to the triplet state of acridinium as the

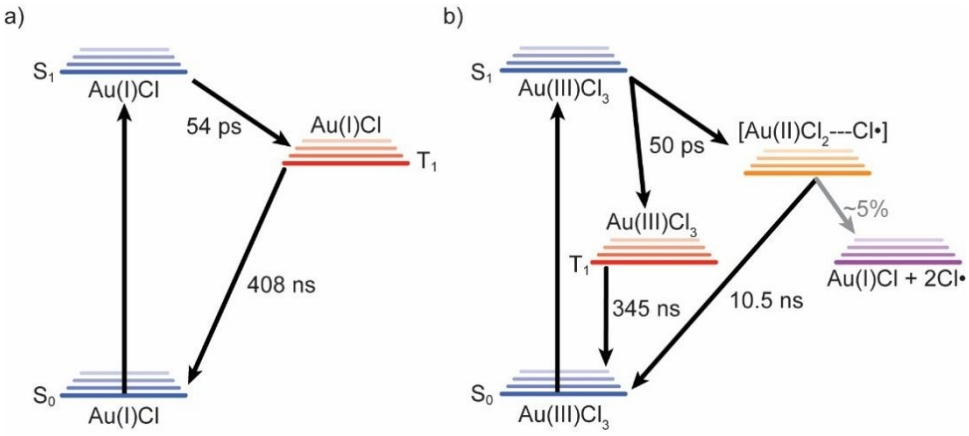

Figure 8 a) Jablonski diagrams depicting the excited state dynamics of [**1a**]$^+$ b) Jablonski diagrams depicting the excited state dynamics of [**2a**]$^+$.

dominant pathway for the decay of the singlet excited state In contrast, the d^8 electronic configuration of Au(III) enables energy transfer from the acridinium singlet excited state to available d-d states of the Au(III) centre.

Conclusions

In summary, we describe a novel mechanism for the visible light-induced photoelimination of chlorine. Our approach relies on the integration of an acridinium chromophore into the photoredox gold platform, enabling electronic excitation of this π^+ system with green light. Although previous work on acridinium derivatives is centred on their photoredox characteristics leading to electron transfer from the excited state,[8, 10] our TA spectroscopic measurements show that direct energy transfer from the excited state of the acridinium moiety to the trivalent gold trichloride facilitates Cl$^\bullet$ elimination as the key photochemical step. Remarkably, our platform is also well-suited for chlorine elimination in the solid state, with negligible deleterious side reactions during photolysis, highlighting the robustness of the system. Finally, the overall reaction can be leveraged to turn on catalysis at gold, as shown for the hydroarylation of alkynes, via photogeneration of the catalytically active mixture.

Author contributions

S. B., E. D. L., K. G. R. contributed equally to this study. E.D.L. carried out the original isolation of [**2a**]$^+$ and surveyed its photoreduction chemistry. S. B. synthesized [**2b**]$^+$ and carried out quantum yield measurement, trapping studies, computations, and catalytic studies. K. G. R. carried out all TA measurements. M. K. assisted with data analysis, validation, and experiment design. F. P. G. and D. G. N. directed the study. All co-authors participated in the preparation of the manuscript.

Conflicts of interest

There are no conflicts to declare.

Data availability

Supporting Information Additional experimental and computational details, crystallographic data for all compounds, and xyz coordinates of the optimized structures are provided in the ESI. Accession Codes Deposition numbers 2521156-2521158 contain the supplementary crystallographic data for this paper. The data can be obtained free of charge via the Cambridge Crystallographic Data Centre (CCDC).

Acknowledgements

The National Science Foundation grants CHE-2154972, CHE-2453754 (F.P.G.) and CHE-2243724 (D.G.N.), the Welch Foundation (A-1423), and Texas A&M University (Arthur E. Martell Chair of Chemistry) (F.P.G.) are gratefully acknowledged for the financial support they provided. Portions of this research were conducted with the advanced computing resources provided by Texas A&M High Performance Research Computing.

Notes and references

1. a) A. Galushchinskiy, R. González-Gómez, K. McCarthy, P. Farràs and A. Savateev, *Energy & Fuels*, 2022, **36**, 4625-4639; b) Z. Li, S. Fang, H. Sun, R.-J. Chung, X. Fang and J.-H. He, *Advanced Energy Materials*, 2023, **13**, 2203019.
2. a) H. B. Gray and A. W. Maverick, *Science*, 1981, **214**, 1201-1205; b) M. D. Brady, R. N. Sampaio, D. Wang, T. J. Meyer and G. J. Meyer, *J. Am. Chem. Soc.*, 2017, **139**, 15612-15615.
3. a) D. G. Nocera, *Inorg. Chem.*, 2009, **48**, 10001-10017; b) L. Troian-Gautier, M. D. Turlington, S. A. M. Wehlin, A. B. Maurer, M. D. Brady, W. B. Swords and G. J. Meyer, *Chem. Rev.*, 2019, **119**, 4628-4683.
4. a) F. David and P. G. David, *J. Phys. Chem.*, 1976, **80**, 579-583; b) D. N. Hendrickson, M. G. Kinnaird and K. S. Suslick, *J. Am. Chem. Soc.*, 1987, **109**, 1243-1244; c) T. S. Teets and D. G. Nocera, *J. Am. Chem. Soc.*, 2009, **131**, 7411-7420; d) T. A. Perera, M. Masjedi and P. R. Sharp, *Inorg. Chem.*, 2014, **53**, 7608–7621; e) R. Fayad, S. Engl, E. O. Danilov, C. E. Hauke, O. Reiser and F. N. Castellano, *J. Phys. Chem. Lett.*, 2020, **11**, 5345-5349; f) D. Gygi, M. I. Gonzalez, S. J. Hwang, K. T. Xia, Y. Qin, E. J. Johnson, F. Gygi, Y.-S. Chen and D. G. Nocera, *J. Am. Chem. Soc.*, 2021, **143**, 6060-6064; g) H. Na, M. B. Watson, F. Tang, N. P. Rath and L. M. Mirica, *Chem. Commun.*, 2021, **57**, 7264-7267.
5. a) T. S. Teets, D. A. Lutterman and D. G. Nocera, *Inorg. Chem.*, 2010, **49**, 3035-3043; b) T. S. Teets, M. P. Neumann and D. G. Nocera, *Chem. Commun.*, 2011, **47**, 1485-1487.
6. a) C. Mongin, I. Pianet, G. Jonusauskas, D. M. Bassani and B. Bibal, *ACS Catal.*, 2015, **5**, 380-387; b) Z. Cao, D. M. Bassani and B. Bibal, *Chem. Eur. J.*, 2018, **24**, 18779-18787.
7. G. Park, M. Karimi, W.-C. Liu and F. P. Gabbaï, *Angew. Chem. Int. Ed.*, 2022, **61**, e202206265.
8. a) S. Fukuzumi, K. Ohkubo, T. Suenobu, K. Kato, M. Fujitsuka and O. Ito, *J. Am. Chem. Soc.*, 2001, **123**, 8459-8467; b) S. Fukuzumi and K. Ohkubo, *Org. Biomol. Chem.*, 2014, **12**, 6059-6071.
9. I. A. MacKenzie, L. Wang, N. P. R. Onuska, O. F. Williams, K. Begam, A. M. Moran, B. D. Dunietz and D. A. Nicewicz, *Nature*, 2020, **580**, 76-80.
10. a) N. A. Romero and D. A. Nicewicz, *Chem. Rev.*, 2016, **116**, 10075-10166; b) K. A. Margrey and D. A. Nicewicz, *Acc. Chem. Res.*, 2016, **49**, 1997-2006.
11. a) L. C. Wilkins, Y. Kim, E. D. Litle and F. P. Gabbaï, *Angew. Chem. Int. Ed.*, 2019, **58**, 18266-18270; b) W.-C. Liu, Y. Kim and F. P. Gabbaï, *Chem. Eur. J.*, 2021, **27**, 6701-6705; c) E. D. Litle and F. P. Gabbaï, *Angew. Chem. Int. Ed.*, 2022, **61**, e202201841; d) W.-C. Liu and F. P. Gabbaï, *Chem. Sci.*, 2023, **14**, 277-283.
12. Y.-Y. Zhu, H.-P. Yi, C. Li, X.-K. Jiang and Z.-T. Li, *Cryst. Growth Des.*, 2008, **8**, 1294-1300. View Article Online DOI: 10.1039/D6SC01586G
13. A. K. H. Al-Sa'ady, C. A. McAuliffe, K. Moss, R. V. Parish and R. Fields, *J. Chem. Soc., Dalton Trans.*, 1984, DOI: 10.1039/DT9840000491, 491-493.
14. A. J. Neel, M. J. Hilton, M. S. Sigman and F. D. Toste, *Nature*, 2017, **543**, 637-646.
15. a) S. Bontemps, G. Bouhadir, K. Miqueu and D. Bourissou, *J. Am. Chem. Soc.*, 2006, **128**, 12056-12057; b) S. Moebs-Sanchez, G. Bouhadir, N. Saffon, L. Maron and D. Bourissou, *Chem. Commun.*, 2008, DOI: 10.1039/b805161e, 3435-3437; c) G. Bouhadir and D. Bourissou, *Chem. Soc. Rev.*, 2016, **45**, 1065-1079.
16. a) J. Hu, B. Xia, D. Bao, A. Ferreira, J. Wan, G. Jones, II and V. I. Vullev, *J. Phys. Chem. A*, 2009, **113**, 3096-3107; b) J. Eberhard, K. Peuntinger, R. Fröhlich, D. M. Guldi and J. Mattay, *Eur. J. Org. Chem.*, 2018, **2018**, 2682-2700.
17. a) M. S. Winston, W. J. Wolf and F. D. Toste, *J. Am. Chem. Soc.*, 2015, **137**, 7921-7928; b) B. Huang, M. Hu and F. D. Toste, *Trends Chem.*, 2020, **2**, 707-720.
18. D. Vesseur, S. Li, S. Mallet-Ladeira, K. Miqueu and D. Bourissou, *J. Am. Chem. Soc.*, 2024, **146**, 11352-11363.
19. a) M. D. Turlington, M. D. Brady and G. J. Meyer, *ACS Appl. Energy Mater.*, 2021, **4**, 745-754; b) S. A. M. Wehlin, L. Troian-Gautier, A. B. Maurer, M. K. Brennaman and G. J. Meyer, *J. Chem. Phys.*, 2020, **153**.
20. a) T. R. Cook, Y. Surendranath and D. G. Nocera, *J. Am. Chem. Soc.*, 2009, **131**, 28-29; b) D. C. Powers, S. J. Hwang, B. L. Anderson, H. Yang, S. L. Zheng, Y. S. Chen, T. R. Cook, F. P. Gabbaï and D. G. Nocera, *Inorg. Chem.*, 2016, **55**, 11815-11820.
21. H. Yang and F. P. Gabbaï, *J. Am. Chem. Soc.*, 2014, **136**, 10866–10869.
22. S. J. Hwang, D. C. Powers, A. G. Maher, B. L. Anderson, R. G. Hadt, S. L. Zheng, Y. S. Chen and D. G. Nocera, *J. Am. Chem. Soc.*, 2015, **137**, 6472-6475.
23. S. Witzel, A. S. K. Hashmi and J. Xie, *Chem. Rev.*, 2021, **121**, 8868-8925.
24. a) S. Sen and F. P. Gabbaï, *Chem. Commun.*, 2017, **53**, 13356-13358; b) A. Franchino, À. Martí, S. Nejrotti and A. M. Echavarren, *Chem. Eur. J.*, 2021, **27**, 11989-11996; c) N. V. Tzouras, A. Gobbo, N. B. Pozsoni, S. G. Chalkidis, S. Bhandary, K. Van Hecke, G. C. Vougioukalakis and S. P. Nolan, *Chem. Commun.*, 2022, **58**, 8516-8519; d) P. Elías-Rodríguez, M. Benítez, J. Iglesias-Sigüenza, E. Díez, R. Fernández, J. M. Lassaletta and D. Monge, *Org. Lett.*, 2024, **26**, 5995-6000.
25. a) M. Alcarazo, *Acc. Chem. Res.*, 2016, **49**, 1797-1805; b) D. You and F. P. Gabbaï, *J. Am. Chem. Soc.*, 2017, **139**, 6843-6846.
26. a) H. J. Kuhn, S. E. Braslavsky and R. Schmidt, *Pure Appl. Chem.*, 2004, **76**, 2105-2146; b) M. Roseau, V. De Waele, X. Trivelli, F. X. Cantrelle, M. Penhoat and L. Chausset-Boissarie, *Helv. Chim. Acta*, 2021, **104**, e2100071.
27. a) K. Kikuchi, C. Sato, M. Watabe, H. Ikeda, Y. Takahashi and T. Miyashi, *J. Am. Chem. Soc.*, 1993, **115**, 5180-5184; b) H. van Willigen, G. Jones and M. S. Farahat, *J. Phys. Chem.*, 1996, **100**, 3312-3316; c) J. W. Verhoeven, H. J. v. Ramesdonk, H. Zhang, M. M. Groeneveld, A. C. Benniston and A. Harriman, *Int. J. Photoenergy*, 2005, **7**, 596840; d) T. Tsudaka, H. Kotani, K. Ohkubo, T. Nakagawa, N. V.

View Article Online
DOI: 10.1039/D6SC01586G

Tkachenko, H. Lemmetyinen and S. Fukuzumi, *Chem. Eur. J.*, 2017, **23**, 1306-1317.
28. G. Jones, M. S. Farahat, S. R. Greenfield, D. J. Gosztola and M. R. Wasielewski, *Chem. Phys. Lett.*, 1994, **229**, 40-46.
29. E. D. Litle, L. C. Wilkins and F. P. Gabbaï, *Chem. Sci.*, 2021, **12**, 3929-3936.
30. M. J. Goodwin, J. C. Dickenson, A. Ripak, A. M. Deetz, J. S. McCarthy, G. J. Meyer and L. Troian-Gautier, *Chem. Rev.*, 2024, **124**, 7379-7464.
31. M. Yan, J. C. Lo, J. T. Edwards and P. S. Baran, *J. Am. Chem. Soc.*, 2016, **138**, 12692-12714.

View Article Online
DOI: 10.1039/D6SC01586G

Data availability

Supporting Information Additional experimental and computational details, crystallographic data for all compounds, and xyz coordinates of the optimized structures are provided in the ESI. Accession Codes Deposition numbers 2521156-2521158 contain the supplementary crystallographic data for this paper. The data can be obtained free of charge via the Cambridge Crystallographic Data Centre (CCDC).